Hou *et al. Carbon Research* (2024) 3:1
https://doi.org/10.1007/s44246-023-00089-7

Carbon Research

ORIGINAL ARTICLE

Open Access

Grinding preparation of 2D/2D g-C_3N_4/BiOCl with oxygen vacancy heterostructure for improved visible-light-driven photocatalysis

Jianhua Hou[1*], Haoyi Wang[1], Rongrong Qin[2], Qikai Zhang[2], Di Wu[3], Zhenhua Hou[3*], Wei Yang[4], Asif Hussain[5], Muhammad Tahir[5], Weiqin Yin[1], Yongcai Zhang[6] and Xiaozhi Wang[1*]

Abstract

A novel 2D/2D g-C_3N_4/BiOCl (CN/BOC) heterojunction photocatalyst was synthesized by grinding appropriate amounts of CN, $Bi(NO_3)_3{\cdot}5H_2O$, glacial acetic acid and KCl at room temperature. The porous CN nanosheets not only facilitate the in situ nucleation and growth of BOC to form thin nanosheets and constitute an intimate contact interface, but also introduce more oxygen vacancies (OVs) in the grinding process. The 2D/2D CN/BOC heterojunction had a good interface and generates a built-in electric field, which can improve the separation of e^- and h^+. The synergistic effect of the heterostructure and OVs made the photocatalyst have significantly better performance than CN and BOC alone under visible light. The most efficient CN/BOC-5 could achieve a tetracycline (TC) degradation rate of 89.8% within 2 h, which was 1.9 and 1.2 times faster than CN and BOC, respectively. It catalyzed the reduction of CO_2 to CO at a rate of 2.00 μmol h^{-1} g^{-1}, 1.1 and 3.2 times faster than CN and BOC, respectively. The mechanism for the photocatalysis of CN/BOC-5 was revealed. It was confirmed that the efficiency of photo-induced carrier separation and visible-light photo-absorption were both considerably increased by the synergistic interaction between OVs and 2D/2D heterojunction. This research may open up new possibilities for the logical design of efficient photocatalysts through combining 2D/2D heterojunctions with OVs for environmental remediation.

Highlights

•Grinding synthesis of 2D/2D BiOCl/g-C_3N_4 heterostructure with oxygen vacancies (OVs).

•The synergistic effect of heterostructure and OVs enabled excellent photoactivity.

•Efficient photocatalytic degradation of organic pollutants and reduction of CO_2.

Keywords Carbon nitride, Photocatalytic, Organic pollutant degradation, Oxygen vacancy, 2D/2D heterostructure

Handling editor: Wenli Zhang

*Correspondence:
Jianhua Hou
jhhou@yzu.edu.cn
Zhenhua Hou
houzhenhualove@126.com
Xiaozhi Wang
xzwang@yzu.edu.cn
Full list of author information is available at the end of the article

Graphical Abstract

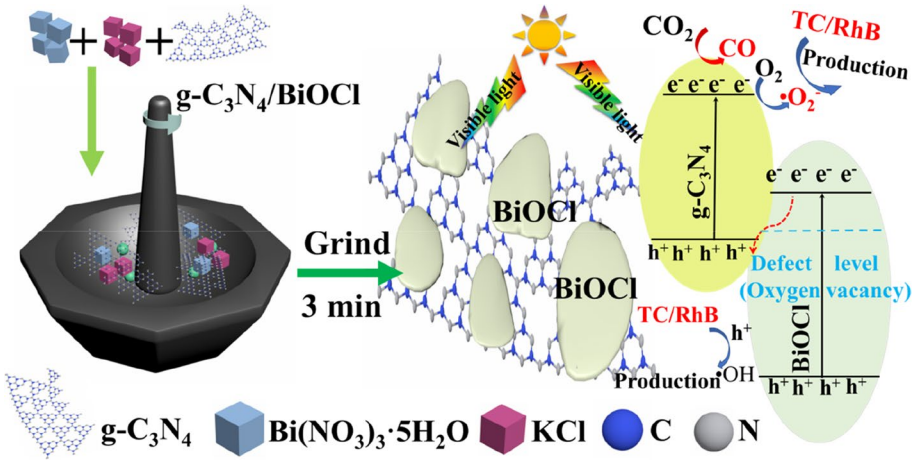

1 Introduction

Most environmental contaminations may be removed using semiconductor photocatalysis, which is considered to be efficient and environmentally sustainable (Chen et al. 2021; Ong et al. 2016). Due to their big specific surface area and distinctive structural properties, two-dimensional (2D) nanosheets have emerged as a novel class of photocatalysts (Chen et al. 2021). The significant two-dimensional anisotropy will lead to the exposure of a large part of internal atoms and will inevitably produce a variety of defects, which can increase light absorption and active sites for photocatalytic reactions (Wang et al. 2018). In particular, the development of efficient and environmentally friendly visible light-driven two-dimensional structure heterojunction materials is considered a potential opportunity to produce very effective photocatalysts (Hu et al. 2019; Shi et al. 2021).

Graphitic carbon nitride (CN) has gained increasing interest as photocatalysts owing to its promising layered structure, visible-light response and narrow band gap (2.7 eV) (Wang et al. 2022a, 2022b, 2022c). However, because of rapid charge recombination and a deficiency in mass diffusion of bulk CN, its photocatalytic performance is far from satisfactory (Ling et al. 2012). Many strategies have been adopted to overcome these shortcomings, for example, exfoliating bulk CN into nanosheet CN can increase specific surface area, enhance electron transfer capability in the in-plane direction, and increase the photo-generated charge carriers' lifetime (Ling et al. 2012; Zhu et al. 2021; Xu et al. 2022). In general, the construction of heterojunction interfaces between semiconductors with matched band structures has been an ideal strategy to promote photogenerated charge migration and separation and enhance the photocatalytic activity and stability (Zhu et al. 2022a; Zhu et al. 2022b). Furthermore, when CN ultrathin nanosheets combine with other layered structure semiconductors (e.g., halogen bismuth oxide) to form 2D/2D heterostructures, their face-to-face interactions will produce a considerable interfacial region, resulting in improved photocatalytic properties (Ong et al. 2016; Wang et al. 2018; Hu et al. 2019).

Bismuth halides have been intensively investigated because of their non-toxic nature, indirect-band gap transition, and open crystalline layered structure (Hou et al. 2019; Wei et al. 2022; Chen et al. 2022a, 2022b). With two layers of chloride ions sandwiching two $[Bi_2O_2]^{2+}$ layers, the BiOCl (BOC) must have an accessible layered structure that provides a sizable space for the polarization of the associated atoms and orbitals. Furthermore, it suppressed the photo-induced electron-hole pair recombination (Wei et al. 2022). Nevertheless, BOC can only be used under UV irradiation due to its large bandgap width, resulting in poor photocatalytic performance under visible light. To date, many methodologies have been used to modify BOC, such as structural control (Hou et al. 2019), introducing oxygen vacancy (Wei et al. 2022; Chen et al. 2022a, 2022b), introduction of specific crystal faces (Li et al. 2022a, 2022b, 2022c), and heterologous hybridization (Hou et al. 2020a, 2020b; Zhou et al. 2021; Zhang et al. 2021a, 2021b, 2021c; Cao et al. 2022; Zhao et al. 2021). Recently, $Bi/BiOCl/Bi_2O_2CO_3$ heterojunction material was synthesized using high-temperature hydrothermal method by Wang et al. (Wang et al. 2022a, 2022b, 2022c), which had higher photocatalytic activity for RhB photodegradation under visible light. However, its photocatalytic activity for the degradation of colorless

non-dye organic contaminants and the reduction of carbon dioxide were still unsatisfactory (Wang et al. 2022a, 2022b, 2022c). So, it is highly attractive to fabricate a novel 2D structure using BOC and a narrow band gap semiconductor, for further enhancing the visible-light photocatalytic performance of BOC (Zhang et al. 2021a, 2021b, 2021c). However, construction of 2D/2D heterostructure with efficient photocatalytic activity via green and easy methods remains a challenge.

Herein, employing a simple grinding technique as shown in Fig. 1, we have created oxygen vacancy CN-BOC heterostructure nanosheets with high visible-light-driven photocatalytic activity. The 2D/2D heterostructures with small thickness have an intimate surface to interact with reactants. It also reduces the transfer route of photo-generated charge carriers and realizes a higher electron-hole pair separation rate (Ling et al. 2012; Zhu et al. 2021). Improved electron-hole separation efficiency and optical absorption can lead towards the higher visible-light photocatalytic efficiency due to the collective effect of both oxygen vacancies (OVs) and heterojunction in CN-BOC nanosheets. The photocatalytic performances of all composites were tested by the degradation of rhodamine B (RhB), which is a common dye and widely applied in industry. In addition, tetracycline, as the most common antibiotic contaminant, is also used as a degradation target to determine the photocatalytic performance of composite materials. The photocatalytic performance of 2D/2D CN-BOC heterostructures in the degradation of tetracycline (TC) and rhodamine B (RhB) as well as the reduction of CO_2 was significantly superior to that of single CN and BOC. This work will provide a simple and green method to develop oxygen vacancy-rich 2D/2D heterostructures for improving photo-generated charge carriers' separation for efficient photocatalytic activity.

2 Experimental section

2.1 Material synthesis

2.1.1 Preparation of CN (g-C_3N_4) nanosheets

After proper mass ratio of thiourea and dicyandiamide was mixed and heated at 550 °C for 2 hours (the heating rate was 5 °C min^{-1}), the obtained yellow bulk g-C_3N_4 sample (20 g) was fed into a tubular furnace via N_2 carrier gas in 8% ethanol solution and heated at 500 °C for 2 hours (5 °C min^{-1}), washed, dried and ground.

2.1.2 Preparation of BiOCl (BOC)

Twenty mmol $Bi(NO_3)_3{\cdot}5H_2O$, 0.4 mL glacial acetic acid and 20 mmol KCl were ground for 3 minutes, washed three times with pure water, and dried at 60 °C.

2.1.3 Preparation of CN/BiOCl-X photocatalyst

Different mass ratios of CN (0.2, 0.5, 1.0 g), 20 mmol $Bi(NO_3)_3{\cdot}5H_2O$, 0.4 mL glacial acetic acid and 20 mmol KCl were ground for 3 minutes and then washed three times with pure water. Finally, the composite products were dried at 60 °C, and named CN/BOC-2, CN/BOC-5, CN/BOC-10, respectively.

2.2 Photocatalytic tests

2.2.1 Photocatalytic organic pollutant degradation tests

The Xenon lamp (power = 500 W, and wavelength (λ) > 420 nm optical filter) was used as a visible light simulator. The Rhodamine B (RhB, 10 mg L^{-1}) and Tetracycline (TC, 10 mg L^{-1}) were taken as simulated contaminants. Twenty mg of the synthesized material was mixed with 50 ml of the contaminants' aqueous solution and stirred in the dark for 2 h to reach an adsorption-desorption equilibrium. Lastly, samples were then taken every 30 min in the light. Each degradation experiment was repeated three times. The average result of the three repeated trials was used as the final result, and the estimated error was signified by the error bar in the figures.

2.2.2 Photocatalytic CO_2 reduction by gas-solid method

A Pyrex quartz reactor in a closed circular system was used for photocatalytic carbon dioxide reduction experiments. A xenon lamp with a power of 300 W (CEL-HXF300, China Education Au-light, Beijing) was used as the visible energy source. The 20 mg of photocatalyst material was evenly distributed on the quartz reaction stage, and 1 mL of deionized water was inoculated into

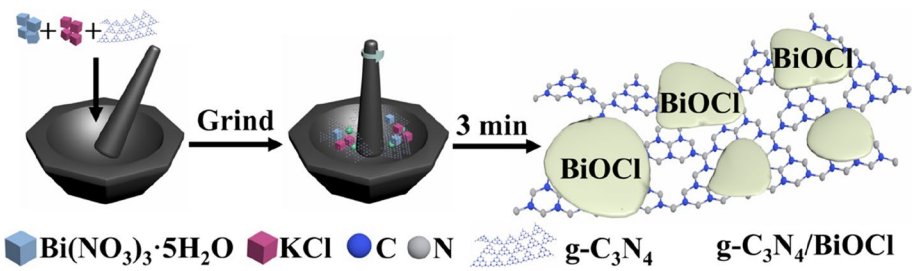

Fig. 1 Synthesis processes of 2D/2D g-C_3N_4/BiOCl heterostructure materials

the reaction system as the electron donor. The reaction system was vacuumed several times, and carbon dioxide gas with a purity of 99.999% was added to the reaction system until the pressure reached 0.08 MPa. In order to ensure that the gas molecules were fully adsorbed, the wind heat pump was used to disperse the gas evenly and keep it for 1 hour. An automatic gas chromatograph (Beijing China Education Au-light Technology CO., LTD., FID2 detector, argon as carrier gas) was used to detect gas products.

2.2.3 Active species experiments

The BQ (1 mmol L^{-1}) and EDTA-2Na (1 mmol L^{-1}) were added into the reaction solution for capturing photogenerated charge carriers such as peroxyl radicals ($\bullet O_2^-$), h^+, and hydroxyl radicals ($\bullet$OH), respectively. The other procedures and operations were similar to the above photocatalytic measurements. Five mg samples were evenly added into 50 mmol L^{-1} DMPO - $\bullet$OH or DMPO-$\bullet O_2^-$ for spin-trapping ESR spectra of CN/BOC-5, respectively.

3 Results and discussion

3.1 Characterization

Figure 2a shows that g-C_3N_4 (CN) has two characteristic peaks at 13.1° and 27.4°, which are crystal plane (100) and crystal plane (002), respectively (Dou et al. 2022). The peaks displayed by BOC at 2θ = 12.0, 24.2, 25.9, 32.6, 33.6, 46.8 and 54.1° in turn agreed with the (001), (002), (101), (110), (102), and (200) crystal planes of BiOCl (Hou et al. 2019). All the diffraction peaks were consistent with the standard card of BiOCl (JCPDS No.06–0249), indicating that BiOCl can be successfully prepared by the solid grinding method. Only one peak of CN appeared in the XRD patterns of the CN/BOC-X composite, which may be attributed to the weak diffraction intensity of CN and its low content, indicating that the presence of CN did not affect the formation of BiOCl in the grinding process. According to the FT-IR spectrum shown in Fig. 2b, some absorption bands of the CN sample can be seen in the range of 1636–1244 cm^{-1}, which may be accredited to the characteristic stretching vibration mode of the C=N heterocycle of g-C_3N_4 (Wu et al. 2021). In addition, a characteristic peak of CN was also found at 816 cm^{-1}, which was considered to be the out-of-plane respiratory vibration peak of the 3-S-triazine unit (Hou et al. 2022). The peak at 521 cm^{-1} was caused by the extended vibration of BI-O in BiOCl, and the peaks at 1632 cm^{-1} and 3436 cm^{-1} were related to the extended vibration modes of adsorbed water molecules and surface hydroxyl groups, respectively (Hou et al. 2021a, 2021b). The above XRD and FT-IR results show that the CN/BOC-X composite was composed of CN and BiOCl.

The absorption edges of pure CN were at approximately 485 nm (Fig. 2c). BOC displayed an absorption edge of about 375 nm, but it demonstrated an absorption tail expanding to the visible region, indicating the existence of OVs (Li et al. 2022a, 2022b, 2022c). Compared with BOC, the light absorption wavelength of the CN/BOC composites gradually redshifted and their band gaps also gradually decreased with the increase in CN content in

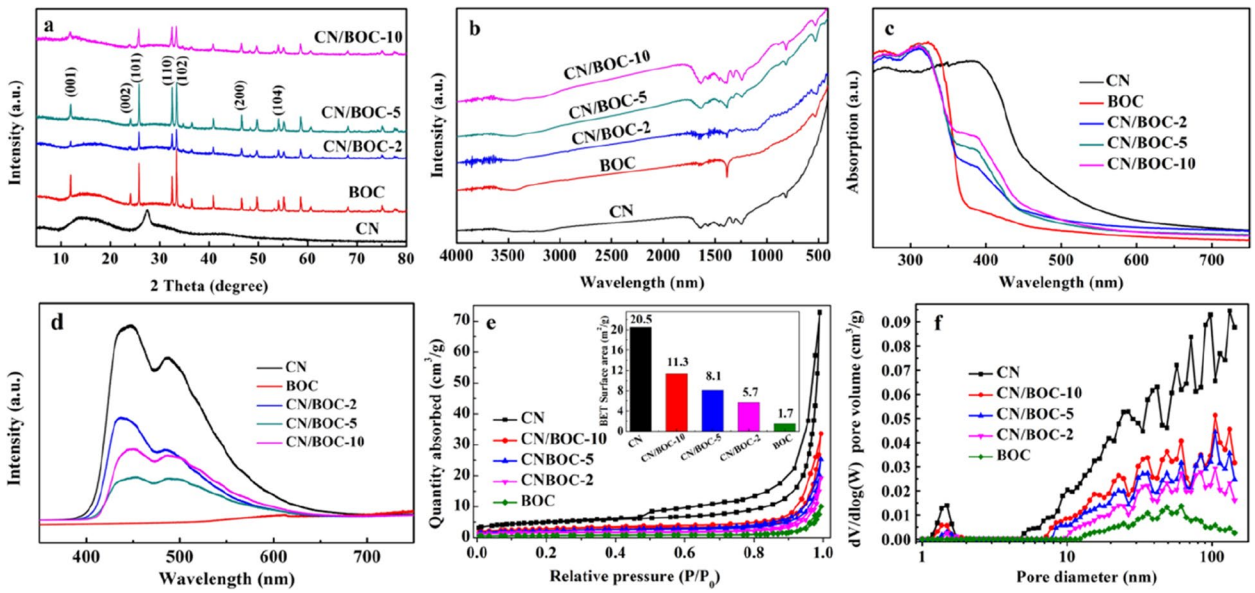

Fig. 2 **a** XRD patterns, **b** FT-IR spectra, **c** UV-Vis DRS, **d** PL, **e** nitrogen adsorption-desorption isotherms (insertion is S_{BET} of the materials), **f** DFT pore size distribution curves of all samples

Fig. S1. Because the CN/BOC composites have a heterojunction structure, they have light absorption ability in the visible light range. Figure 2d shows that CN had the strongest PL intensity, while all CN/BOC-X showed a significant decrease in PL intensity and CN/BOC-5 had the lowest value, indicating that after heterojunctions were formed between CN and BOC, and light-generated charge carriers were effectively separated (Chen et al. 2020). Under the same conditions, there was only a weak PL peak of BOC at 612 nm due to the OVs. Based on N_2 adsorption–desorption isotherms (Fig. 2e), all synthetic materials show typical IV adsorption–desorption isotherms (Hou et al. 2020a, 2020b). CN not only had the highest adsorption volume, but also had a significant hysteresis loop, indicating that it has a larger specific surface area with a rich mesoporous structure. Conversely, the BOC had the lowest adsorption volume among all samples. With the increase of BiOCl in CN/BOC-X, the adsorption amount of N_2 decreased gradually and hysteresis loops became inconspicuous, which may be attributed to the fact that BiOCl nanoparticles filled the mesoporous pores of CN. Experimental results showed that the specific surface areas of CN, CN/BOC-2, CN/BOC-5, CN/BOC-10, and BOC were 20.5, 11.3, 8.1, 5.7, and 1.7 $m^2 g^{-1}$, respectively. Figure 2f shows that CN and CN/BOC-X had micropores in the range of 1.2–2.0 nm, and the porosity gradually decreased with the increase of BOC. Moreover, with the increase of BOC, the minimum mesopore in CN/BOC-X also increased from 7.1 to 9.8 nm. The pure BOC had no micropores and only had a pore size greater than 12 nm. These results indicate that the BOC may enter the porous CN and form an intimate contact heterogeneous interface. The CN/BOC-X with sufficient pore distribution can enable efficient molecular and ion transport for photocatalytic reactions (Hou et al. 2021a, 2021b).

The full survey XPS spectra in Fig. 3a showed the existence of C, N, Bi, O, and C in CN/BOC-5. In Fig. 3b, the main peak of CN/BOC-5 at 288.2 eV can be attributed to the N-C=N bond (Yang et al. 2021) of CN, while the C peak at 284.7 eV may come from the adsorption of impurity carbon by BOC (Shi et al. 2022). It can be seen from Fig. 3c that there are four peaks in the N 1S spectrum of CN at 398.7, 400.1, 401.2, and 404.5 eV, which represent the N in C-N=C, C-N-H, N-$(C)_3$, and π-excitation, respectively (Shi et al. 2022). After combination with BOC, the binding energy of the N element shifted to a higher position by 0.1–0.2 eV, which may be attributed to the adsorption of Bi^{3+} by lone pair electrons in nitrogen (Yang et al. 2021). As can be viewed from Fig. 3d-f, the binding energies of Bi, O, and Cl main peaks all decreased by 0.1 eV in CN/BOC-5 nanosheets compared with pure BOC. However, oxygen vacancies (OVs) appeared at 531.5 eV in the composite materials, the peak

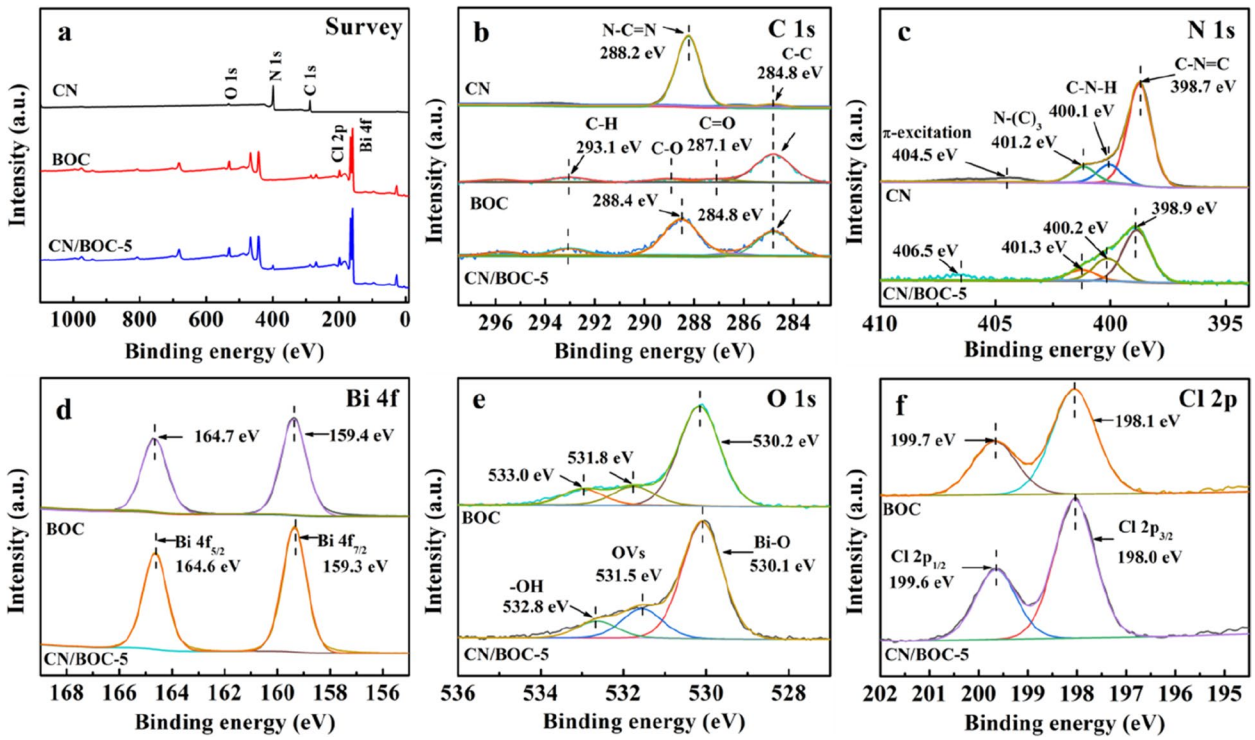

Fig. 3 XPS spectra of CN, BOC, and CN/BOC-5: (**a**) full survey, (**b**) C 1 s, (**c**) N 1 s, (**d**) Bi 4f, (**e**) O1s, and (**f**) Cl 2p

value increased and moved to the lower energy level by 0.3 eV (Wu et al. 2024). The above XPS results indicate that heterojunctions were formed in CN/BOC-5 through the strong interaction between CN and BOC (Zhao et al. 2022).

Figure 4a and Fig. 4d show that CN is a typical aggregated lamellar structure. The SEM (Fig. 4b, e) images of pure BOC show the extremely smooth surface and thick lamelae of BOC crystals. However, when BOC was synthesized in the presence of CN nanosheets, the lamellar thickness was significantly thinner, resulting in the formation of a 2D/2D thinner sheet structure of BOC/CN nanocomposites (Fig. 4c, f). Compared with CN in Fig. 4c, it is confirmed that BOC nanosheets were deposited uniformly on the surface of CN nanosheets of BOC/CN (Fig. 4f), and the original shape of CN was not obviously changed. According to Fig. 4g, CN/BOC showed a good contact interface between CN and BOC, and the lattice spacings of about 0.28 nm and 0.34 nm corresponded to (110) and (101) crystal planes of BOC, respectively (Wang et al. 2021). In addition, some lattice defects (marked by blue ovals) can be clearly seen, which may be caused by the existence of oxygen vacancies or defects on the crystal surface (Zhang et al. 2021a, 2021b, 2021c). The EDX elemental mapping (Fig. 4h-m) indicated that Bi and Cl had the same shape and distribution, which overlapped with a part of the mapping images of C, N and O. This further confirms the formation of BOC/CN heterojunction. The possible mechanism is that N atoms in porous g-C_3N_4 nanosheets may coordinate with Bi^{3+} ions (Chen et al. 2020), and then BOC grows in situ on the surface or in the porous channel structure of g-C_3N_4. Finally, the gradually growing BOC's small-sized nanoparticles form the structure of nanosheets. These results also indicated that CN and BOC were successfully coupled and formed a good contact interface. The 2D/2D structure of the CN/BOC heterojunction has a good interface and generates an induced electric field, which can promote the e^- and h^+ separation (Wang et al. 2018; Zhang et al. 2021a, 2021b, 2021c; Li et al. 2022a, 2022b, 2022c; Chen et al. 2020).

3.2 Photocatalytic performance

The degradation of tetracycline by the prepared catalysts is shown in Fig. 5a. Before light irradiation, dark adsorption for 60 min made the catalysts get into the adsorption equilibrium state. The TC adsorption capacity of pure BOC was greater than that of CN. It may be attributed to the hydroxyl functional group of BOC's interaction with these oxygen-containing groups in TC via hydrogen bonding (Guo et al. 2020; Dai et al. 2021). For CN/BOC-X composites, their TC adsorption amounts were obviously higher than pure CN and BOC. After visible light exposure for 120 min, the elimination rate of TC by CN/BOC-X was higher than that by CN and BOC alone. For example, the TC degradation rates of CN/BOC-2, CN/BOC-5, and CN/BOC-10 reached 78.3, 89.8, and 86.2%, respectively, which were obviously higher than

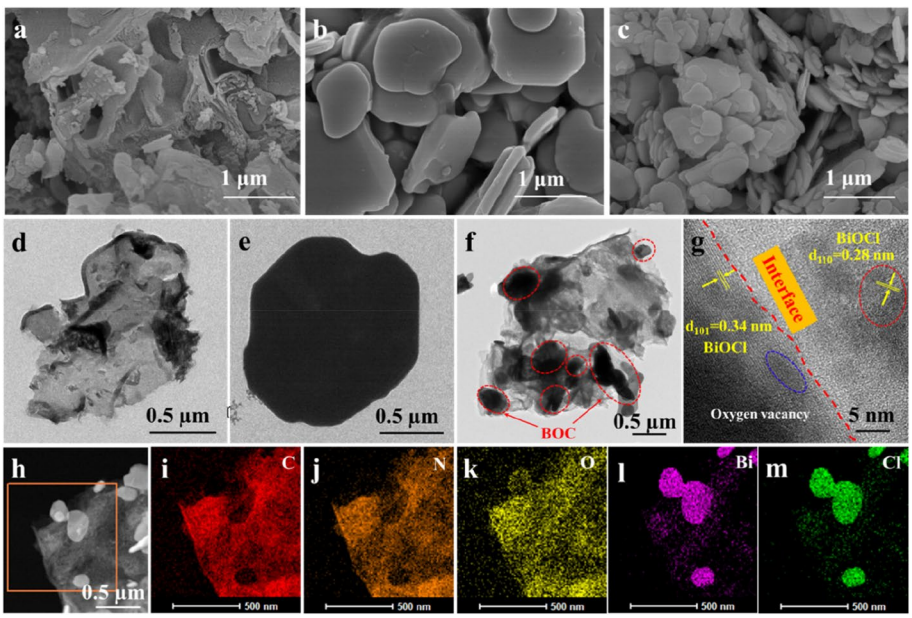

Fig. 4 SEM images of (**a**) CN, (**b**) BOC, and (**c**) CN/BOC-5; TEM images of (**d**) CN, (**e**) BOC, and (**f**) CN/BOC-5; (**g**) HRTEM image of CN/BOC-5, (**h**-**m**) STEM, and elemental mapping images of CN/BOC-5

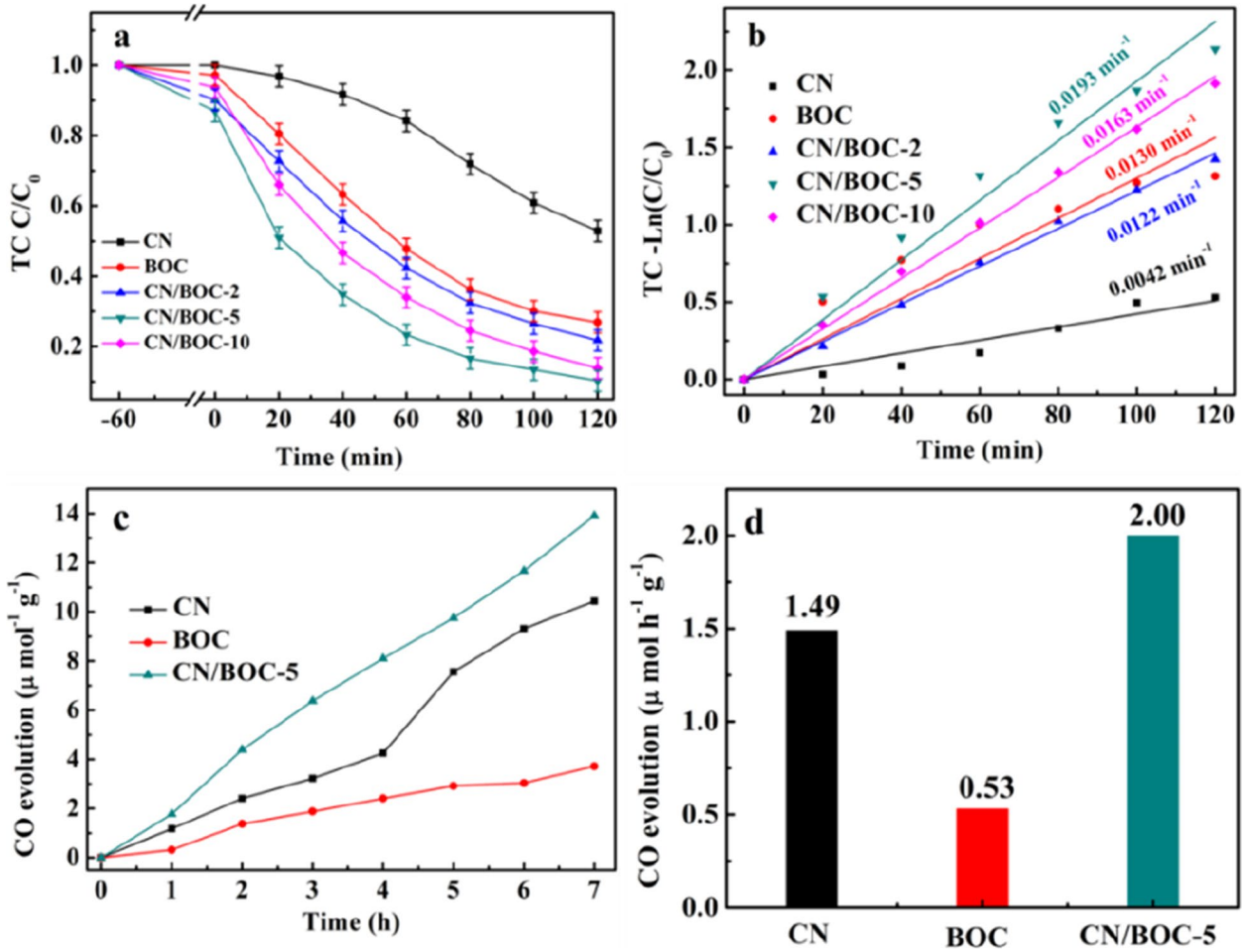

Fig. 5 **a** Photocatalytic degradation of TC by all samples and (**b**) plots of -ln(C/C$_0$) vs. irradiation time for the TC degradation reactions in (a), (**c**) yield curve of CO_2 reduction to CO and (**d**) rate diagram of CO_2 reduction to CO of CN, BOC and CN/BOC-5

those of single CN (47.1%) and BOC (73.1%), respectively. In addition, the optimal degradation rate of CN/BOC-5 (0.0193 min^{-1}) was 4.6 and 1.5 times higher than that of single CN (0.0042 min^{-1}) and BOC (0.0130 min^{-1}), respectively (Fig. 5b). The reason may be that, compared with the single photocatalyst, CN/BOC-5 with 2D/2D heterostructure and oxygen-rich vacancies can enhance the space charge separation at the interface and improve the photocatalysis activity (Wang et al. 2018; Zhu et al. 2021; Hou et al. 2021a, 2021b).

In addition, the degradation of RhB also showed that the optimal CN/BOC-5 can catalyze the photo-degradation of 88% RhB after 60 min, much higher than 15% of CN and 67% of BOC (Fig. S1a). The absorption spectra of RhB solution during degradation were measured using UV-Vis spectrometer (Fig. S5). As can be seen from Fig. S5, CN/BOC-5 adsorbed 12% of RhB under 1 hour darkness and showed excellent catalytic activity in the degradation of RhB under visible light irradiation. The RhB degradation reaction rate constant of CN/BOC-5 was 0.0295 min^{-1}, which was 18.4 times that of CN (0.0016 min^{-1}) and 1.8 times that of BOC (0.0162 min^{-1}). Cycling performance is an important index to evaluate the stability of a photocatalyst. As shown in Fig. S4, CN/BOC-5 can keep high catalytic performance over 5 cycles of photocatalytic degradation of RhB. Compared with the first cycle, the degradation rate of RhB in the fifth cycle only decreased by about 10%. This may be due to the loss of CN/BOC-5 photocatalyst during its recovery after the cycling tests. In conclusion, CN/BOC-5 had excellent photocatalytic performance in the degradation of various organic pollutants.

As shown in Fig. 5c, d, the samples were also tested for photocatalytic CO_2 reduction by the gas-solid method. After 7 hours of light exposure, 2D/2D CN/BOC-5 heterostructure had the highest yield of CO

(2.00 μmol h^{-1} g^{-1}), which was 1.3 times that of single CN (1.49 μmol h^{-1} g^{-1}) and 3.8 times that of single BOC (0.53 μmol h^{-1} g^{-1}). Thus, the CO generation rate was significantly increased after CN and BOC combination, indicating that 2D/2D interface plays a significant part in CO_2 transformation (Zhu et al. 2021; Hou et al. 2021a, 2021b). Furthermore, the activity of CN/BOC-5 in photocatalytic organic pollutant degradation and carbon dioxide reduction is comparable or superior to those of BiOCl (Zhou et al. 2021), porous g-C_3N_4 (Tang et al. 2022), and even BiOCl-g-C_3N_4 composite (Zhang et al. 2019), etc., as listed in Tables S2 and S3.

3.3 Mechanism

The 2D/2D CN/BOC heterojunction materials show excellent photocatalytic activity, and the involved mechanism needs to be further explored. Figure 6a shows that the ElS radius of the CN/BOC-5 composite is the smallest, indicating that its charge transfer resistance is the smallest. The excellent interfacial transfer efficiency of CN/BOC-5 will improve the separation efficiency of e^--h^+ pairs (Hou et al. 2022). The calculation of equivalent series resistance (ESR) is shown in Fig. S6. It is evident from Table S1 that CN/BOC-5 and CN/BOC-10 had a similar ESR, but it was much lower than that of pure CN, pure BOC and CN/BOC-2. The Rct of pure BOC and CN were in turn 3.7 and 1.5 times that of CN/BOC-5, indicating that CN/BOC-5 had better electron diffusion pathways. Figure 6b shows that all samples showed stable transient photo-current response characteristics, and the photo-current density of the CN/BOC-X heterojunction materials was higher than that of single CN and BOC. The photo-current density of CN/BOC-5 was the most significant, which indicates that appropriate heterojunction composition has a positive effect on further improving the photocatalytic activity. According to the direct electron paramagnetic resonance (EPR) test results in Fig. 6c, the peak at g = 2.003 became more intense with the coupling BOC with CN, which proved the presence of oxygen vacancies in the CN/BOC-X (Li et al. 2022a, 2022b, 2022c). This is consistent with the results of HRTEM and XPS. A new defect level was added by introducing OVs, which led to the enhanced photo-absorption efficiency (Chen et al. 2022a, 2022b). The surface OVs can act as electron trapping sites and inhibit the recombination of e^--h^+, thus playing an important role in the charge transfer process of the CN/BOC heterostructure (Li et al. 2022a, 2022b, 2022c).

As shown in Fig. 6d, with the addition of BQ or EDTA-2NA, the photocatalytic activity of CN/BOC-5 decreased significantly, indicating that $\bullet O_2^-$ and h^+ played significant roles in the photocatalytic reactions (Ji et al. 2023; Liu et al. 2022). Nevertheless, the addition of IPA had a moderate influence on the photocatalytic efficiency, indicating that the production of •OH radical is not sufficient. Furthermore, when DMPO was used as a spin capture agent, the characteristic ESR signal peaks of •OH radical and $\bullet O_2^-$ free radicals were detected (Fig. 6e, f).

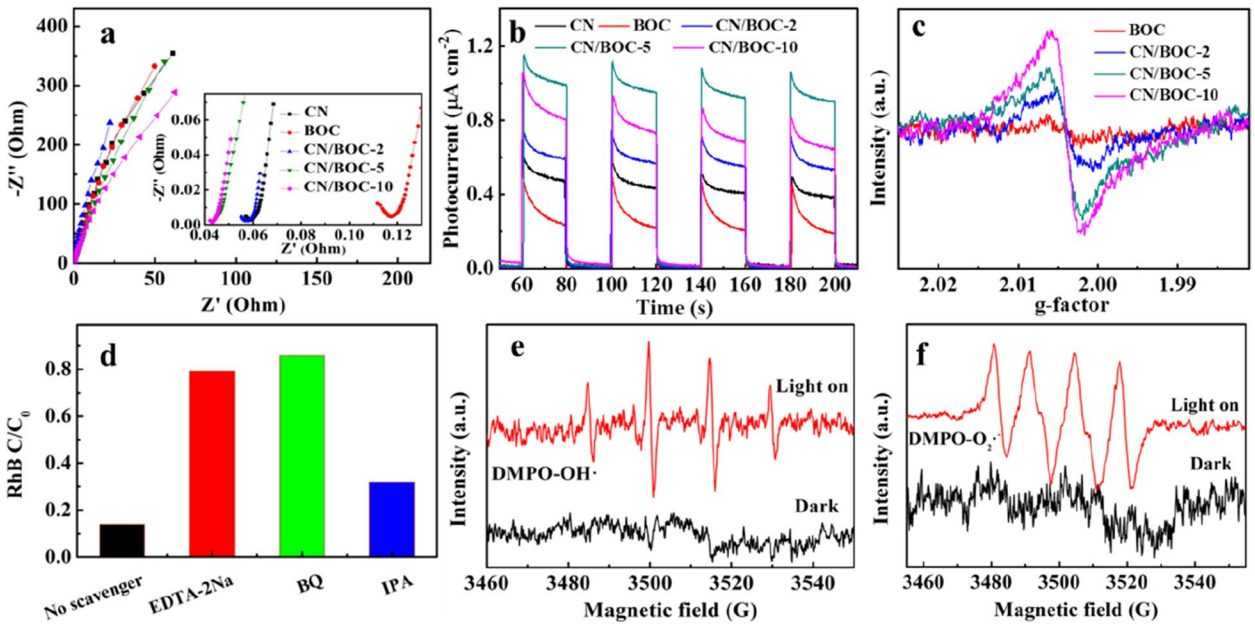

Fig. 6 (**a**) EIS, (**b**) photocurrent responses curves, (**c**) EPR spectra of prepared samples, (**d**) free radical capture experiment results, (**e**) ESR signals of DMPO-•OH, (**f**) ESR signals of DMPO-•O_2^- for CN/BOC-5

Therefore, the synergistic effect of CN/BOC heterojunction materials can produce both •OH and $•O_2^-$, which greatly improves the photocatalytic efficiency.

The valence band (VB) and conduction band (CB) potentials of g-C_3N_4 and BiOCl were calculated as follows:

$$E_{CB} = X - E_e - 0.5E_g \quad (1)$$

$$E_{VB} = E_{CB} + E_g \quad (2)$$

Where X (absolute electronegativity) of g-C_3N_4 is 4.73 eV (Wu et al. 2022), X of BiOCl is 6.36 eV (Zhou et al. 2021), E_e is the energy of free electrons on the hydrogen scale (4.5 eV), and E_g is 2.3 eV for CN and 3.2 eV for BOC (Fig. S1). The calculated E_{CB} and E_{VB} were −0.97 and 1.33 eV for g-C_3N_4, 0.26 and 3.46 eV for BiOCl, respectively. CN has an appropriate bandgap and can be excited by visible light. Meanwhile, because the defect levels caused by OVs can cause visible-light excitation of BOC, BOC could also be photoexcited to produce e^- and h^+ (Li et al. 2022a, 2022b, 2022c). According to the conduction band (VB) potential of CN and the valence band (VB) potential of BOC, $•O_2^-$ ($O_2/•O_2^-$, −0.33 V vs. NHE) and •OH/OH^- (1.99 eV vs. NHE) can be generated, which was also confirmed by the above-mentioned trapping experiments and ESR tests (Hou et al. 2019). In the process of photo-reducing reaction of CO_2, the edge potential of CB of CN is less than the standard redox potential of CO_2/CO (−0.53 eV). The potential difference is sufficient for the thermodynamic conditions (Dou et al. 2022). The possible mechanism is shown in Fig. 7. In the Z-scheme structure, the electrons on CB of BOC and holes on VB of CN are combined, whereas the holes on VB of BOC and electrons on CB of BOB are retained, thus maintaining the higher oxidation and reduction ability of the composite photocatalyst. Therefore, the electrons in the CB of CN may contribute electrons to oxygen to generate $•O_2^-$ radicals, whereas the holes in the VB of BOC will further generate •OH radicals, which is justified by the test results as shown in Fig. 5d, f. In particular, the electronic structure of BOC is affected by its surface OVs and a new defect energy level is formed (Li et al. 2022a, 2022b, 2022c), which may render photoelectrons to transfer to OVs. As a result, OVs serve as e^--traps and slow down the recombination of e^--h^+ pairs, which results in the increased lifetime of photo-induced carriers (Chen et al. 2022a, 2022b; Wu et al. 2022; Chen et al. 2022a, 2022b). In addition, CN/BOC heterojunction forms a strong built-in electric field at the 2D/2D interface, which is favorable to the efficient separation of photogenerated electron-hole pairs (Hou et al. 2021a, 2021b; Li et al. 2022a, 2022b, 2022c; Chen et al. 2020; Hou et al. 2021a, 2021b). Therefore, the obtained CN/BOC-OVs heterojunction with a 2D/2D structure is endowed with synergistic effects (Wang et al. 2022a, 2022b, 2022c; Perumal et al. 2023), which

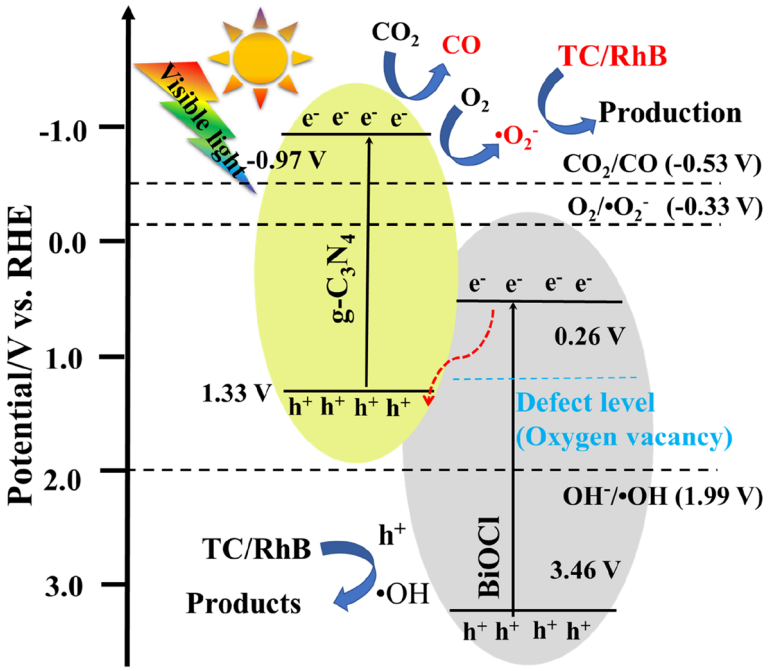

Fig. 7 Photocatalytic mechanism diagram of the CN/BOC-OV heterojunction

can significantly improve the photocatalytic oxidation/reduction performance. It is superior to some other g-C_3N_4, BiOCl, and heterojunction photocatalysts (as shown in Table S2 and S3).

4 Conclusion

CN/BOC heterojunction photocatalyst with a 2D/2D structure was prepared by a one-step grinding method. This solid-phase reaction introduced abundant OVs in the CN/BOC heterojunction, which could increase the visible-light absorption. The 2D/2D structure enhances bonding at the heterojunction interface and generates an induced internal electric field, which can improve the e^- and h^+ separation. The photoluminescence and transient photocurrent measurements showed that the recombination of photo-generated carriers is suppressed due to heterojunction. In addition, free radical capture and spin capture ESR spectra confirmed that $\bullet O_2^-$, •OH and h^+ participate in the degradation reactions of organic contaminants. The interfacial OVs could provide more photo-generated charge carriers to contribute to the CO_2 reduction reaction. The synergistic effect of the heterostructure and OVs makes the CN/BOC photocatalyst significantly more efficient than CN and BOC alone under visible light. The results showed that the rhodamine B degradation rate by the optimum CN/BOC-5 heterojunction was 18.4 times that by pure CN and 1.8 times that by pure BOC. Photocatalytic degradation of tetracycline and reduction of carbon dioxide showed similar results. This study provides an easy route for preparing 2D/2D CN/BOC heterojunctions with oxygen vacancies for photocatalytic environmental remediation.

Abbreviations

2D/2D	Two-dimension/ two-dimension
CN/BOC	g-C_3N_4/BiOCl
OVs	Oxygen vacancies
$\bullet O_2^-$	Superoxide radical
•OH	Hydroxyl radical
h^+	Hole
TC	Tetracycline
RhB	Rhodamine B
EIS	Electrochemical impedance spectroscopy
EPR	Electron Paramagnetic Resonance

Supplementary Information

The online version contains supplementary material available at https://doi.org/10.1007/s44246-023-00089-7.

Additional file 1: Materials and Characterization of Experimental section. **Fig. S1** plots of $(ahv)^{1/2}$ versus hv of all samples. **Fig. S2** SEM images of (a) BOC, (b) CN/BOC-2, (c) CN/BOC-5 and (d) CN/BOC-10. **Fig. S3** (a) Photocatalytic degradation and (b) $-\ln(C/C_0)$ of RhB. **Table S2** Comparison of photocatalytic degradation of CN/BOC-5 (g-C_3N_4/ BiOCl-5) with other photocatalysts. **Table S3** Comparison of CO_2 reduction performance of CN/BOC-5 (g-C_3N_4/ BiOCl-5) with other g-C_3N_4-based systems.

Acknowledgments

The authors are grateful for the financial support by the National Natural Science Foundation of China (51602281), Innovative Science and Technology Platform Project of Cooperation between Yangzhou City and Yangzhou University, China (No. YZ202026308), Yangzhou University self-made experimental equipment special fund (YZUZZ2022-13), Yangzhou University High-end Talent Support Program and the "Qinglan Project" of Jiangsu University.

Authors' contributions

Jianhua Hou developed the methodology, acquired funding, and prepared the manuscript. Haoyi Wang, Rongrong Qin and Qikai Zhang synthesized and characterized the materials and conducted data analyses. Di Wu, Wei Yang and Zhenhua Hou supervised the study and revised the manuscript. Muhammad Tahir and Asif Hussain revised the manuscript. Weiqin Yin, Yongcai Zhang and Xiaozhi Wang supervised the study and reviewed and edited the manuscript. All the authors were involved in the completion of the manuscript.

Funding

National Natural Science Foundation of China (51602281), Innovative Science and Technology Platform Project of Cooperation between Yangzhou City and Yangzhou University, China (No. YZ202026308), Yangzhou University self-made experimental equipment special fund (YZUZZ2022–13), Yangzhou University High-end Talent Support Program and the "Qinglan Project" of Jiangsu University.

Availability of data and materials

Data will be made available on request.

Declarations

Competing interests

The authors declare no competing financial interest.

Author details

[1]College of Environmental Science and Engineering, Yangzhou University, Yangzhou 225000, China. [2]Beijing Xinfeng Aerospace Equipment Co., Ltd, Beijing 100854, China. [3]Jiangxi Xinda Hangke New Materials Technology Co., Ltd, Nanchang 330096, China. [4]Beijing System Design Institute of Electro-Mechanic Engineering, Beijing 100005, China. [5]Department of Physics, Division of Science & Technology, University of Education, Lahore, Pakistan. [6]School of Chemistry and Chemical Engineering, Yangzhou University, Yangzhou 225009, China.

Received: 3 March 2023 Revised: 8 November 2023 Accepted: 24 December 2023
Published online: 16 January 2024

References

Cao J, Cen W, Jing Y, Du Z, Chu W, Li J (2022) P-doped BiOCl for visible light photodegradation of tetracycline: An insight from experiment and calculation. Chem Eng J 435:134683

Chen C, Jiang T, Hou J, Zhang T, Zhang G, Zhang Y, Wang X (2022a) Oxygen vacancies induced narrow band gap of BiOCl for efficient visible-light catalytic performance from double radicals. J Mater Sci Technol 114:240–248

Chen R, Ren Z, Liang Y, Zhang G, Dittrich T, Liu R, Liu Y, Zhao Y, Pang S, An H, Ni C, Zhou P, Han K, Fan F, Li C (2022b) Spatiotemporal imaging of charge transfer in photocatalyst particles. Nature 610:296–301

Chen Y, Wang F, Cao Y, Zhang F, Zou Y, Huang Z, Ye L, Zhou Y (2020) Interfacial oxygen vacancy engineered two-dimensional g-C_3N_4/BiOCl Heterostructures with boosted photocatalytic conversion of CO_2. ACS Appl Energy Mater 3:4610–4618

Chen Y, Xu M, Wen J, Wan Y, Zhao Q, Cao X, Ding Y, Wang Z, Li H, Bian Z (2021) Selective recovery of precious metals through photocatalytic. Nat Sustain 4:618–626

Dai D, Qiu J, Li M, Xu J, Zhang L, Xu J, Zhang L, Yao J (2021) Construction of two-dimensional BiOI on carboxyl-rich MIL-121 for visible-light photocatalytic degradation of tetracycline. J Alloys Compd 872:159711

Dou Q, Hou J, Hussain A, Zhang G, Zhang Y, Luo M, Wang X, Cao C (2022) One-pot synthesis of sodium-doped willow-shaped graphitic carbon nitride for improved photocatalytic activity under visible-light irradiation. J Colloid Interf Sci 624:79–87

Guo Y, Yan C, Wang P, Rao L, Wang C (2020) Doping of carbon into boron nitride to get the increased adsorption ability for tetracycline from water by changing the pH of solution. Chem Eng J 387:124136

Hou J, Dai D, Wei R, Wu X, Wang X, Tahir M, Zou J (2019) Narrowing the band gap of BiOCl for the hydroxyl radical generation of photocatalytic under visible light. ACS Sustain Chem Eng 7:16569–16576

Hou J, Dou Q, Jiang T, Yin J, Liu J, Li Y, Wang X (2020a) BiOCl/cattail carbon composites with hierarchical structure for enhanced photocatalytic activity. Sol Energy 211:1263–1269

Hou J, Jiang T, Wang X, Zhang G, Zou J, Cao C (2021a) Variable dimensional structure and interface design of g-C_3N_4/BiOI composites with oxygen vacancy for improving visible-light photocatalytic properties. J Clean Prod 287:125072–125080

Hou J, Tu X, Wu X, Shen M, Wang X, Wang C, Wang G (2020b) Remarkable cycling durability of Lithium-sulfur batteries with interconnected mesoporous hollow carbon Nanospheres as high sulfur content host. Chem Eng J 401:126141–126151

Hou J, Yang M, Dou Q, Chen Q, Wang X, Hu C, Paul R (2022) Defect engineering in polymeric carbon nitride with accordion structure for efficient photocatalytic CO_2 reduction and H_2 production. Chem Eng J 450(4):138425

Hou J, Zhang T, Jiang T, Wu X, Zhang Y, Tahir M, Hussain A, Luo M, Zou J, Wang X (2021b) Fast preparation of oxygen vacancy-rich 2D/2D bismuth oxyhalides-reduced graphene oxide composite with improved visible-light photocatalytic properties by solvent-free grinding. J Clean Prod 328:129651

Hu X, Zhang Y, Wang B, Li H, Dong W (2019) Novel g-C_3N_4/$BiOCl_xI_{1-x}$ nanosheets with rich oxygen vacancies for enhanced photocatalytic degradation of organic contaminants under visible and simulated solar light. Appl. Catal. B. 256:117789

Ji Z, Cai R, Ye W, Lu P, Dong CL, Huang YC, Yang D (2023) Confined Fe single atomic sites on (100) plane of anatase TiO_2 nanofibers boost white LED driven Fenton-like norfloxacin degradation. J Clean Prod 382:135161

Li Q, Ren J, Hao YJ, Li YL, Wang XJ, Liu Y, Su R, Li FT (2022c) Insight into reactive species-dependent photocatalytic toluene mineralization and deactivation pathways via modifying hydroxyl groups and oxygen vacancies on BiOCl. Appl. Catal. B. 317:121761

Li S, Cai M, Liu Y, Wang C, Lv K, Chen X (2022a) S-scheme photocatalyst TaON/Bi_2WO_6 nanofibers with oxygen vacancies for efficient abatement of antibiotics and Cr(VI): intermediate eco-toxicity analysis and mechanistic insights. Chin J Catal 43:2652–2664

Li S, Cai M, Wang C, Liu Y, Li N, Zhang P, Li X (2022b) Rationally designed Ta_3N_5/BiOCl S-scheme heterojunction with oxygen vacancies for elimination of tetracycline antibiotic and Cr(VI):performance, toxicity evaluation and mechanism insight. J Mater Sci Technol 123:177–190

Ling G, Ng S, Ong W (2012) Tailor-engineered 2D Cocatalysts: harnessing Electron-hole redox center of 2D g-C_3N_4 Photocatalysts toward solar-to-chemical conversion and environmental purification. Adv. Funct. Mater 32:2111875

Liu Y, Wang X, Ye W, Butenko DS, Lu P, Chen Q, Yang D (2022) FeOx nanoclusters decorated TiO2 for boosting white LED driven photocatalytic Fenton-like norfloxacin degradation. Sep Purif Technol 303:122194

Ong W, Tan L, Ng Y, Yong S, Chai S (2016) Graphitic carbon nitride (g-C_3N_4)-based photocatalysts for artificial photosynthesis and environmental remediation: are we a step closer to achieving sustainability? Chem Rev 116:7159–7329

Perumal K, Shanavas S, Ahamad T, Karthigeyan A, Murugakoothan P (2023) Construction of Ag_2CO_3/BiOBr/CdS ternary composite photocatalyst with improved visible-light photocatalytic activity on tetracycline molecule degradation. J Environ Sci 125:47–60

Shi X, Huang Y, Bo Y, Duan D, Wang Z, Cao J, Zhu G, Ho W, Wang L, Huang T, Xiong Y (2022) Highly selective photocatalytic CO_2 Methanation with water Vaporon single-atom platinum-decorated defective carbon nitride. Angew Chem Int Ed 61:202203063

Shi Y, Li J, Mao C, Liu S, Wang X, Liu X, Zhao S, Liu X, Huang Y, Zhang L (2021) Van Der Waals gap-rich BiOCl atomic layers realizing efficient, pure-water CO_2-to-CO photocatalytic. Nat Commun 12:1–10

Tang J, Wang J, Tang L, Feng C, Zhu X, Yi Y, Feng H, Yu J, Ren X (2022) Preparation of floating porous g-C_3N_4 photocatalyst via a facile one-pot method for efficient photocatalytic elimination of tetracycline under visible light irradiation. Chem Eng J 430:132669

Wang L, Ma X, Huang G, Lian R, Huang J, She H, Wang Q (2022a) Construction of ternary CuO/$CuFe_2O_4$/g-C_3N_4 composite and its enhanced photocatalytic degradation of tetracycline hydrochloride with persulfate under simulated sunlight. J Environ Sci 112:59–70

Wang L, Yin H, Wang S, Wang J, Ai S (2022c) Ni^{2+}-assisted catalytic one-step synthesis of bi/BiOCl/$Bi_2O_2CO_3$ heterojunction with enhanced photocatalytic activity under visible light. Appl Catal B 305:121039

Wang M, Tan G, Ren H, Lv L, Xia A (2022b) Enhancement mechanism of full-solar-spectrum catalytic activity of g-C_3N_{4-x}/bi/Bi_2O_2 $(CO_3)_{1-x}$ $(Br, I)_x$ heterojunction: the roles of plasma bi and oxygen vacancies. Chem Eng J 430:132740

Wang M, Wang B, Xie B, Li N, Xu Q, Li H, Lu J (2021) Ultrathin two-dimensional BiOCl with oxygen vacancies anchored in three-dimensional porous g-C_3N_4 to construct a hierarchical Z-scheme heterojunction for the photocatalytic degradation of NO. Ind Eng Chem Res 61:317–329

Wang Q, Wang W, Zhong L, Liu D, Cao X, Cui F (2018) Oxygen vacancy-rich 2D/2D BiOCl-g-C_3N_4 ultrathin heterostructure nanosheets for enhanced visible-light-driven photocatalytic activity in environmental remediation. Appl. Catal. B. 220:290–302

Wei S, Zhong H, Wang H, Song Y, Jia C, Anpo M, Wu L (2022) Oxygen vacancy enhanced visible light photocatalytic selective oxidation of benzylamine over ultrathin Pd/BiOCl nanosheets. Appl. Catal. B. 305:121032

Wu C, Xue S, Qin Z, Nazari M, Yang G, Yue S, Bao J (2021) Making g-C_3N_4 ultrathin nanosheets active for photocatalytic overall water splitting. Appl. Catal. B. 282:119557

Wu C, Zuo H, Zhang S, Zhao S, Du H, Yan Q (2022) A novel strategy to construct a direct Z-scheme bi@$Bi_2O_2CO_3$/g-C_3N_4 heterojunction catalyst via PDA electronic bridge. Sep Purif Technol 294:121242

Wu X, Yan L, Qin R, Zhang Q, Yang W, Wang X, Zhang Y, Luo M, Hou J (2024) Enhanced photocatalytic performance by $Bi_2O_2CO_3$/$Bi_4O_5Br_2$/reduced graphene oxide Z-scheme heterojunction via a one-pot room-temperature synthesis. J Environ Sci 138:418–427

Xu L, Li L, Yu L, Jimmy CY (2022) Efficient generation of singlet oxygen on modified g-C_3N_4 photocatalyst for preferential oxidation of targeted organic pollutants. Chem Eng J 431:134241

Yang T, Mao X, Zhang Y, Wu X, Wang L, Chu M, Pao C, Yang S, Xu Y, Huang X (2021) Coordination tailoring of cu single sites on C_3N_4 realizes selective CO_2 hydrogenation at low temperature. Nat Commun 12:1–9

Zhang G, Liu Y, Zheng S, Sun Z (2021b) Efficient removal of formaldehyde by diatomite decorated with BiOCl/TiO_2 under visible-light irradiation: effects of key preparation parameters. Adv Powder Technol 32:4364–4372

Zhang R, Niu S, Xiang J, Zheng J, Jiang Z, Guo C (2021c) Band-potential fluctuation in C_3N_4/BiOCl hetero-junction for boosting photo-catalytic activity. Sep Purif Technol 261:118258

Zhang T, Chen L, Jiang T, Hou J, Zhang G, Hussain A (2021a) Chemical precipitation synthesis of $Bi_{0.7}Fe_{0.3}OCl$ nanosheets via Fe (III)-doped BiOCl for highly visible light photocatalytic performance. Mater Today Commun 26:102145

Zhang X, An D, Feng D, Liang F, Chen Z, Liu W, Yang Z, Xian M (2019) In situ surfactant-free synthesis of ultrathin BiOCl/g-C_3N_4 nanosheets for enhanced visible-light photodegradation of rhodamine B. Appl Surf Sci 476:706–715

Zhao DX, Lu GP, Cai C (2021) Efficient visible-light-driven Suzuki coupling reaction over CO-doped BiOCl/Ce-doped $Bi_2O_2CO_3$ composites. Green Chem 23:1823–1833

Zhao J, Ji M, Chen H, Weng Y, Zhong J, Li Y, Wang S, Chen Z, Xia J, Li H (2022) Interfacial chemical bond modulated $Bi_{19}S_{27}Br_3$/g-C_3N_4 Z-scheme heterojunction for enhanced photocatalytic CO_2 conversion. Appl. Catal. B. 307:121162

Zhou P, Shen Y, Zhao S, Li G, Cui B, Wei D, Shen Y (2021) Synthesis of clinoptilolite-supported BiOCl/TiO_2 heterojunction nanocomposites with highly-enhanced photocatalytic activity for the complete degradation of xanthates under visible light. Chem Eng J 407:126697

Zhu B, Cheng B, Fan J, Ho W, Yu J (2021) G-C_3N_4-based 2D/2D composite heterojunction photocatalyst. Small Struct 2:2100086
Zhu Y, Sikandaier A, Zhang Y, Wang X, Du B, Xue J, Yang D (2022a) FeOx@ FeP heterostructure: surface phosphorization toward efficient photocatalytic Fenton-like norfloxacin removal. Environmental Functional Materials 1(3):230–238
Zhu Y, Zhuang Y, Wang L, Tang H, Meng X, She X (2022b) Constructing 0D/1D Ag_3PO_4/TiO_2 S-scheme heterojunction for efficient photodegradation and oxygen evolution. Chinese J Catal 43:2558–2568

Publisher's Note